Ceramics International 50 (2024) 35725–35733

Contents lists available at ScienceDirect

Ceramics International

journal homepage: www.elsevier.com/locate/ceramint

High-strength low-*k* glass–ceramic composite covers for 6G communication mobile devices

Ji Yeon Kim [a,1], Seok Won Choi [a,1], Kwan Sik Park [a,1], Yong-yi Kim [b], Taehong Kim [b], Sang Bong Lee [b], Jongsu Lee [b], Seok Eun Kwon [c], Young-Kook Lee [a], Do-Kyun Kwon [c,**], Sang-Jin Lee [d,***], Yong Soo Cho [a,*]

[a] Department of Materials Science and Engineering, Yonsei University, Seoul, 03722, Republic of Korea
[b] Samsung Electronics Co., Ltd., Suwon, Gyeonggi-do, 16677, Republic of Korea
[c] Department of Materials Science and Engineering, Korea Aerospace University, Gyeonggi-do, 10540, Republic of Korea
[d] Department of Advanced Materials Engineering, Mokpo National University, Muan, 58554, Republic of Korea

ARTICLE INFO

Handling Editor: Dr P. Vincenzini

Keywords:
Phone cover
Cordierite
Stabilized zirconia
High strength
Low dielectric constant

ABSTRACT

Ceramic-based back covers are commercially utilized as a high-end option for the physical protection of mobile phones. Herein, an unprecedented composite structure consisting of a cordierite ($2MgO{\cdot}2Al_2O_3{\bullet}5SiO_2$) glass–ceramic strengthened with yttria-stabilized zirconia (YSZ) fillers is introduced as a protective back cover, specifically for next-generation communication mobile phones additionally requiring a low dielectric constant at gigahertz frequencies. Crystallization sequence was rather complicated with the involvements of multiple crystalline phases, α- and μ-cordierite, tetragonal and monoclinic ZrO_2, and $ZrSiO_4$, depending on the glass and composite compositions. This unique approach effectively induced the best mechanical performance for the 10 wt% YSZ/glass–ceramic structure, despite the low sintering temperature of 1050 °C, with the highest Vickers hardness of ~9.2 GPa and flexural strength of ~196.8 MPa attained for the optimal composite. Although effective dielectric constant of the composites depended on the relative contents of the evolved crystalline phases, overall dielectric constant was kept low due to the utilization of cordierite glass as the main component.

1. Introduction

High-strength ceramic materials have long been considered to overcome the limitations of the mechanical properties of typical refractory ceramics in numerous physical applications [1–3]. Yttria-stabilized zirconia (YSZ) is one of the best materials for realizing high mechanical strength and toughness [4–6]. One unusual commercial application of YSZ is as the back cover of mobile phones with a thickness of ~0.5–0.6 mm, although its wide implementation is restricted owing to its high price and technical difficulty of fabrication process. The back cover is intended to physically protect the mobile phone against mechanical stress from various fracture-inducing sources, such as dropping, scratching, and shock, with outward attractions. As long as ceramic covers are considered, YSZ will inevitably be selected for its remarkable mechanical properties. However, its high dielectric constant (k) limits its application beyond 5th generation (5G) communication, which requires suitable dielectric properties at microwave frequencies. As anticipated, 6G mobile networks enable virtual connections among machines, objects, and devices everywhere with higher data speeds, ultralow latency, and massive network capability. Supporting components such as substrates and covers, as well as active chip devices, must be designed to meet the requirements of these unprecedented network environments. In particular, a high k value can impede proper communication through the back cover in wireless networks.

In this regard, we introduce unique high-strength low-k ceramic materials for next-generation mobile phones expected to work for next-generation wireless communications. Specifically, the back cover must have a low k of ideally less than 6 in the gigahertz (GHz) range, not

* Corresponding author.
** Corresponding author.
*** Corresponding author.
E-mail addresses: dkwon@kau.ac.kr (D.-K. Kwon), lee@mokpo.ac.kr (S.-J. Lee), ycho@yonsei.ac.kr (Y.S. Cho).
[1] These authors contributed equally to this work.

https://doi.org/10.1016/j.ceramint.2024.06.390
Received 12 April 2024; Received in revised form 12 June 2024; Accepted 27 June 2024
Available online 28 June 2024

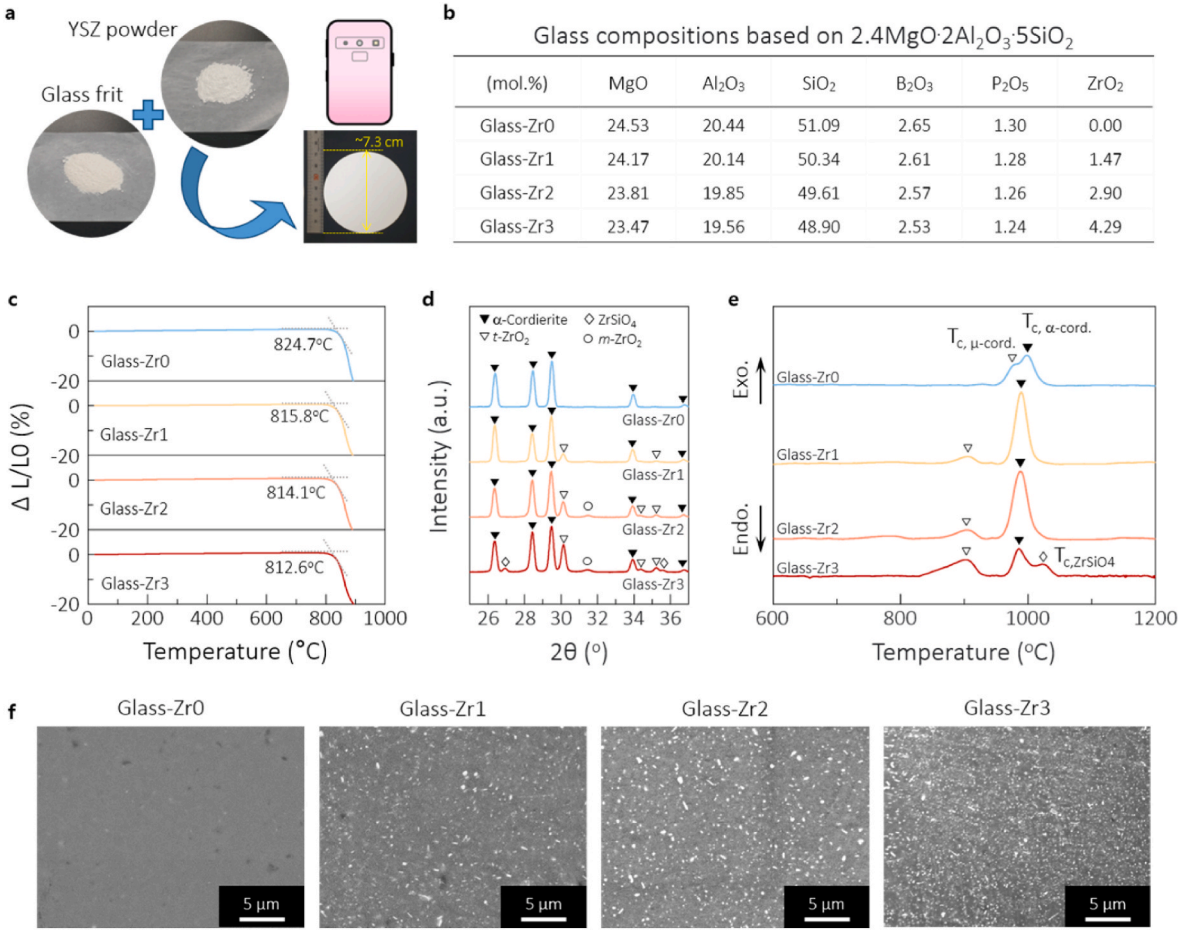

Fig. 1. (a) Schematic of the formation of composite samples from cordierite glass frit and YSZ filler for the mobile phone cover. (b) Glass compositions based on excess MgO–cordierite, $2.4MgO{\cdot}2Al_2O_3{\cdot}5SiO_2$, containing minor constituents of B_2O_3 and P_2O_5 with variable contents of ZrO_2 as nucleating agent. (c) TMA curves of the glasses, Glass-Zr0, Glass-Zr1, Glass-Zr2, and Glass-Zr3, demonstrating the on-set temperature of densification depending on the relative content of ZrO_2 in glasses. (d) XRD patterns of the cordierite-based glasses, showing the formation of crystalline cordierite as major phase. (e) DTA curves of the glasses with exothermic peaks of crystallization depending on the glass chemistry. (f) Surface SEM photographs of the glass samples densified at 1050 °C for 2h.

achievable using zirconia-based materials having k~25. Because ceramic compounds alone do not likely meet the requirements, the composite approach is inevitably chosen. There is no composite reported particularly for aiming proper high-frequency dielectric properties with exceptional mechanical robustness. The dielectric requirement is quite challenging because modifying the composition of YSZ materials to lower k by more than half can significantly deteriorate the mechanical properties. Accordingly, a new material system must be developed to satisfy the required dielectric properties while maintaining high mechanical properties. Herein, cordierite ($2MgO{\cdot}2Al_2O_3{\cdot}5SiO_2$)-based glass–ceramic is newly suggested as an alternative material for the high-strength back cover that provides excellent dielectric and mechanical characteristics sufficient for commercialization with proper compositional modifications.

Cordierite is a recognized material with promising characteristics, including low thermal expansion, low k, and high thermal shock resistance, making it suitable for electronic packaging applications [7–9]. However, crystalline cordierite possesses poor mechanical strength and toughness, and achieving a high fired density is difficult even at its high sintering temperature of >1300 °C [10,11]. Owing to its limited mechanical properties, compositing cordierite has been widely investigated to boost its fracture strength and toughness by controlling phase evolution and microstructural features [12–14]. For example, composites of crystalline cordierite toughened with zirconia have demonstrated substantially enhanced strength and toughness depending on the zirconia content and sintering temperature [15–17].

This work proposes for the first time a high-strength, low-permittivity material, i.e., a unique composite system consisting of cordierite glass and stabilized zirconia, which forms a glass–ceramic structure incorporating a dispersed YSZ filler. In particular, zirconia is involved in the glass chemistry as a nucleating agent in controllable amounts to help toughen the glass–ceramic structure with the precipitated zirconia phase. This combination of cordierite glass–ceramics with a zirconia filler is novel, as only ceramic/ceramic composites of cordierite ceramic and zirconia have been reported thus far. In contrast to typical ceramic/ceramic composites of cordierite ceramic and zirconia, the sintering temperature of the proposed glass–ceramic/ceramic composites is only 1050 °C in contrast to 1200–1400 °C for reported ceramic/ceramic composites [18,19]. The phase evolution and its resulting influence on the dielectric and mechanical properties are investigated by varying the zirconia contents in the glasses and composites. Crystallizable glasses with ceramic fillers have been extensively studied for ceramic substrate applications requiring a low temperature firing [20–23]. The optimized values, Vickers hardness of 9.2 GPa and flexural strength of 196.8 MPa, for the 4.29 mol.% ZrO_2-containing glass with 10 wt% YSZ are very competitive compared to the corresponding values reported for cordierite-based composites even when a much lower sintering temperature of 1050 °C is used. The reported performance will be compared with our best values in terms of suitability for the proposed applications. Origin of our mechanical excellency is discussed in terms of phase evolution and its influence on mechanical properties.

2. Experimental section

The glass compositions were based on excess-MgO cordierite, i.e., $2.4MgO{\cdot}2Al_2O_3{\bullet}5SiO_2$ with B_2O_3, P_2O_5, and ZrO_2 as minor components. Depending on the zirconia content in the glass, four different glass compositions were used, designated as Glass-Zr0 (with 0 mol.% ZrO_2 in glass), Glass-Zr1 (with 1.47 mol.% ZrO_2), Glass-Zr2 (with 2.90 mol.% ZrO_2), and Glass-Zr3 (with 4.29 mol.% ZrO_2). The reagent raw materials, i.e., $MgCO_3$ (99 %, Aldrich Co.), Al_2O_3 (99.9 %, High Purity Chemical), SiO_2 (99.8 %, Ferro Corp.), H_3BO_3 (99.9 %, High Purity Chemical), $NH_4H_2PO_4$ (99.8 %, High Purity Chemical), and ZrO_2 (99 %, Aldrich Co., for Glass-Zr1, Glass-Zr2, and Glass-Zr3 only), were admixed by ball-mixing for 16 h and then melted at 1550 °C in a Pt crucible for the four glasses. The resulting melt was quenched by a roller to form a quenched glass. The glass was ball-milled to obtain glass frits with average particle sizes of 2.3–2.8 μm. The glass frits were then ball-mixed with 0, 5, 10, 15, or 20 wt% commercial YSZ powder (8 wt% yttria–zirconia, Sigma-Aldrich) for 16 h in ethanol. After drying the slurry at 120 °C, the powder mixture was further mixed with a 1.5 wt% polyvinyl alcohol (PVA) aqueous binder and uniaxially pressed at ~100 MPa to form pellets with a diameter of 15 mm. The pellets were sintered at 1050 °C for 2 h after binder burnout at 550 °C. Pellets with different dimensions were used for various dielectric and mechanical measurements.

Crystal structures of the sintered pellets were primarily analyzed using an X-ray diffractometer (X'pert PRO, PANalytical, The Netherlands) in the 2θ scan range of 5–60°. Surface microstructural images of the composite samples were obtained using a field-emission scanning electron microscopy (FE-SEM, JEOL-7610F, JEOL, Japan). High-resolution transmission electron microscopy (HR-TEM, JEM-ARM200F, JEOL, Japan) was used to observe microstructures with the assistance of a standard focused ion beam (FIB, Crossbeam 350, ZEISS, Germany) technique for sample preparation. The densification behaviors of the glasses were determined using a thermomechanical analyzer (TMA, TMA4000 SA, Bruker AXS, USA). To understand the crystallization paths, differential thermal analysis (DTA) curves for the selected samples were recorded up to 1200 °C at a fixed heating rate of 5 °C/min using a thermogravimetric analyzer (SDT Q600, TA Instruments, USA).

The Vickers hardness H values of the finely polished samples were measured using a microhardness tester (HM-122, Mitutoyo, Japan) with a diamond pyramid tip. Each sample was indented multiple times under a loading force of 9.8 N for 10 s to obtain average values. The flexural strength and modulus were evaluated by the common three-point bending method using a universal mechanical testing machine (ST-1000, SALT, Korea) at a loading rate of 0.5 mm/min for bar-type samples with dimensions of 40 × 20 × 2 mm. The flexural strength σ_f was calculated using the equation $\sigma_f = 3FL/2bd^2$, where F is the maximum load, L is the span width between the two supports, b is the width of the sample, and d is the sample thickness. Meanwhile, equation $E = FL^3/4ybd^3$ was used to estimate the flexural modulus E where y is the deflection. The fracture toughness K_{1c} of the composite samples was also determined by the indentation-fracture method performed under an applied load varying between 2.94 and 19.6 N, using the relation of $K_{1c} = \beta(PH)^{1/2}/4C$, where β is $0.025(E/H)^{0.4}$, P is the applied indentation load, and C is the Palmqvist crack length [24]. The relative dielectric permittivity k at microwave frequencies was measured using the post-resonator method with parallel conductive plates, as guided by Hakki and Coleman, using a network analyzer (E8364B, Agilent Technologies Inc. Santa Clara, CA, USA) [25]. The loss tangent tanδ and quality factor $Q \times f$ at microwave frequencies were also determined using the transmission resonant cavity method with a silver cavity and quartz support [26]. The measurement frequencies for the post-resonator and transmission resonant cavity methods were ~9 and ~14 GHz, respectively.

3. Results and discussion

Fig. 1(a) shows a photograph of the glass–ceramic/ceramic composite sample formed via the densification and crystallization process from the mixed raw materials, cordierite glass frit and commercial YSZ powder, which is targeted for mobile phone covers. Four cordierite glasses with different contents of ZrO_2 were selected and are hereafter labeled with following the Zr contents, namely, Glass-Zr0, Glass-Zr1, Glass-Zr2, and Glass-Zr3, as listed in Fig. 1(b). The glasses were based on excess-MgO cordierite composition, $2.4MgO{\cdot}2Al_2O_3{\bullet}5SiO_2$ with minor constituents of B_2O_3 and P_2O_5. Only the relative content of ZrO_2 was changed in the glasses while all other molar ratios are maintained. All the compositions were successfully melted under the same melting condition at 1550 °C. Fig. S1 of Supplementary Material shows a photograph of transparent pelletized glasses after melt-quenching, confirming that clear cordierite-based glasses formed for the glass compositions. Using excess MgO beyond the stoichiometric amount for cordierite was intended to help facilitate the crystallization with easy melting and reduce the weight of the glass (owing to the low density of MgO itself) [27,28]. The proposed system is uniquely based on a glass–ceramic/ceramic composite system, which differs from typical high-strength ceramic/ceramic composites, e.g., cordierite/zirconia [29], SiC/zirconia [30], and mullite/zirconia [31], particularly in terms of its densification mechanism. Our system enables the use of a low sintering temperature of 1050 °C for the composites because of the low-temperature softening of the glasses involved as a major constituent. Fig. 1(c) shows the densification behavior of the four glasses with increasing temperature, as determined by TMA measurements. The on-set temperature of densification was found to decrease gradually from 824.7 to 812.6 °C as the relative content of ZrO_2 in glasses was raised up to 4.29 mol.%. The earlier densification with more ZrO_2 in the glasses may be associated with the relative reduction in the glass-former components of SiO_2 and B_2O_3. The incorporation of small contents of B_2O_3 and P_2O_5 into cordierite glass is extensively studied to facilitate stable formation of glass network with controllable crystallization [32–34]. B_2O_3 is a part of the glass former while P_2O_5 mainly influences the nucleation of cordierite phase. For example, the presence of P_2O_5 results in earlier crystallization of α-cordierite [35,36]. Note that the glasses contain identical amounts of B_2O_3 and P_2O_5 relative to the cordierite glass components.

Fig. 1(d) shows the X-ray diffraction (XRD) patterns of the glasses containing different contents of ZrO_2 after firing at 1050 °C for 2 h in the 2θ range of 25 to 37°, which was selected for easier comparison of the evolved crystalline phases depending on the content of ZrO_2. The extended patterns in the broader 2θ range of 5 to 60° are available in Fig. S2. The formation of a glass–ceramic structure is evident with distinct peaks of α-cordierite phase as a major constituent in all the glasses. Notably, tetragonal zirconia (t-ZrO_2) phase started to appear with the addition of ZrO_2 and became apparent with the higher contents of ZrO_2 added to the glass. The t-ZrO_2 phase was assumed to be precipitated out upon firing along with the crystallization of cordierite. Note that the as-prepared glasses were amorphous with no crystalline peak as seen in the XRD patterns of Fig. S3. Similarly, the presence of the ZrO_2 phase was reported in other cordierite-based glass systems after forming glass–ceramics, where the ZrO_2 phase was observed even at a small concentration in the glass [37,38]. Moreover, only the Glass-Zr3 sample exhibited minor peaks corresponding to zircon ($ZrSiO_4$) phase, indicating that some of ZrO_2 reacted with SiO_2 to form zircon phase. It should be also mentioned that peak traces of monoclinic zirconia (m-ZrO_2) were found in the glasses of Glass-Zr2 and Glass-Zr3.

Crystallization behavior of the glasses was examined by the DTA as seen in Fig. 1(e), where distinct exothermic peaks of crystallization are evidently seen depending on the glass chemistry. Two distinguishable crystallization peaks of μ-cordierite and α-cordierite in the DTA were identified in the Glass-Zr3 based on the extra XRD patterns of Fig. S4 where μ-cordierite phase was dominantly observed at a low temperature

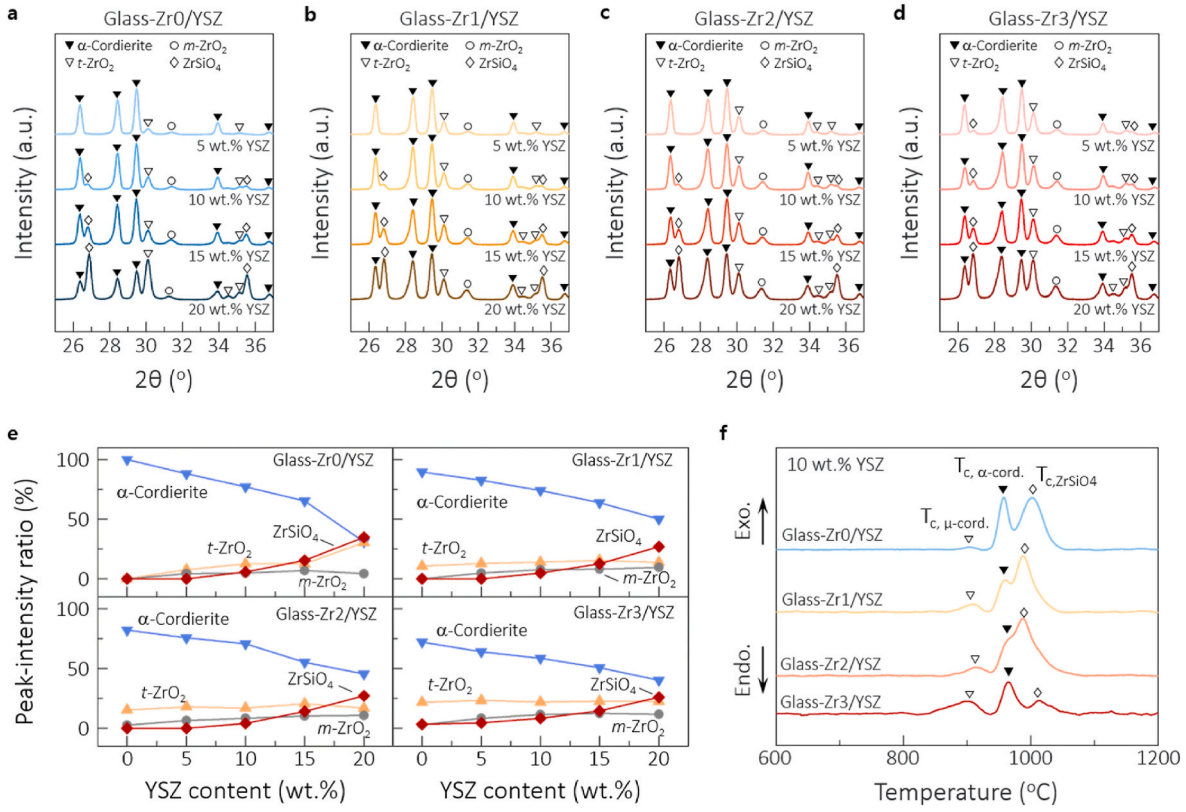

Fig. 2. (a–d) XRD patterns of the composite samples sintered at 1050 °C for 2 h, which consist of (a) Glass-Zr0, (b) Glass-Zr1, (c) Glass-Zr2, and (d) Glass-Zr3 with different contents of YSZ filler up to 20 wt% YSZ. (e) Variations in the relative content of each crystalline phase with increasing the YSZ content for the glasses, which were estimated by comparing the relative ratios of the strongest intensity peaks in XRD patterns. (f) DTA curves of the composite samples in the case of 10 wt% YSZ fillers added to the glasses, clearly demonstrating the dependence of the distinct exothermic peaks of crystallization on the composite compositions and temperature.

of 900 °C and then disappeared at 950 °C as exemplified in the cases of Glass-Zr0 and Glass-Zr3. It indicates that the transformation of μ-cordierite to α-cordierite phase happens upon firing. The transition to α-cordierite is well recognized as a typical route to stable cordierite crystallization [39,40]. It should be mentioned that the incorporation of ZrO_2 in the glass induced the earlier crystallization of the intermediate μ-cordierite compared to the case of Glass-Zr0, as expected from the role of ZrO_2 as a nucleating agent [41,42]. As another crystalline phase, $ZrSiO_4$ was observed at ~1024 °C only for the Glass-Zr3, which is expected from the XRD pattern of the Glass-Zr3. Fig. 1(f) presents surface SEM images of the glasses sintered at 1050 °C for 2 h. Fully densified microstructures are seen as expected from earlier densification and later crystallization of the glasses as confirmed from the previous TMA and DTA curves. The increased white precipitates of presumable ZrO_2 phase is noticeable on the surface of the glass–ceramic samples with more ZrO_2 in the glasses.

Hereafter, composite samples consisting of the glass frits with different YSZ fillers up to 20 wt% are characterized. Fig. 2(a–d) shows the XRD patterns of the densified composites at 1050 °C for 2 h in the narrow 2θ range of 25–37°. The XRD patterns in the extended 2θ range of 5 to 60° are presented in Fig. S5. Evolution of crystalline phases depended on the type of glass and the content of YSZ filler. For easy comparison, Fig. S6 shows the rearranged XRD patterns of the composites with the same content of filler for different glasses. There are four different crystalline phases, α-cordierite, *t*-ZrO_2, *m*-ZrO_2, and zircon, involved in the composites. The relative contents of the crystalline phases in each composite were roughly estimated by comparing the intensity of the strongest peak of each phase relative to the added peak intensities of all the crystalline peaks, as presented in Fig. 2(e) demonstrating the evolution of each phase with increasing the YSZ filler in the composites. The strongest peaks correspond to (100) plane of α-cordierite at 2θ~10.4°, (101) plane of *t*-ZrO_2 at 2θ~30.1°, (111) plane of *m*-ZrO_2 at 2θ~31.4°, and (200) plane of zircon at 2θ~26.8°.

The relative content of α-cordierite was found to decrease substantially as the YSZ filler increased irrespective of the glasses, which accompanies more crystallization of $ZrSiO_4$ phase. Zircon is known to be a reaction product of cordierite ceramics and zirconia in ceramic/ceramic composites at high temperatures >1300 °C [43,44]. However, zircon formation at the low temperature of 1050 °C has never been reported thus far. Nonetheless, zircon is likely to easily form when SiO_2 is supplied by the glasses because the cordierite glass and the surface of YSZ particles are in intimate contact during the densification process, owing to the viscous movement of the melted glass above ~800 °C. In particular, the strong presence of zircon was evident in the composites containing more than 10 wt% YSZ, presumably indicating that the extended contact areas with more fillers facilitated the formation of extensive zircon phase. Interestingly, *t*-ZrO_2 phase was not proportionally increased with the higher contents of YSZ fillers in the glasses (except for the case of Glass-Zr0), while *m*-ZrO_2 phase was found as an accompanying phase with the incorporation of YSZ. As the commercial YSZ filler is mainly tetragonal (as seen in the XRD pattern of Fig. S7), the presence of *m*-ZrO_2 suggests the occurrence of phase transformation from the tetragonal to monoclinic structure [45,46]. Fig. 2(f) shows the DTA curves of the composites of the glasses with 10 wt% YSZ. All the curves demonstrate a distinct crystallization peak of $ZrSiO_4$ after the crystallization peak of α-cordierite phase. The earlier exothermic peak corresponds to the crystallization of μ-cordierite as confirmed in the XRD patterns of Fig. S8 for composites densified at the lower temperatures of 900 and 950 °C.

Fig. 3(a and b) shows the plots of variations in fired density and linear shrinkage of the composites with changing the YSZ content for each glass. As expected, the absolute values of density tended to increase

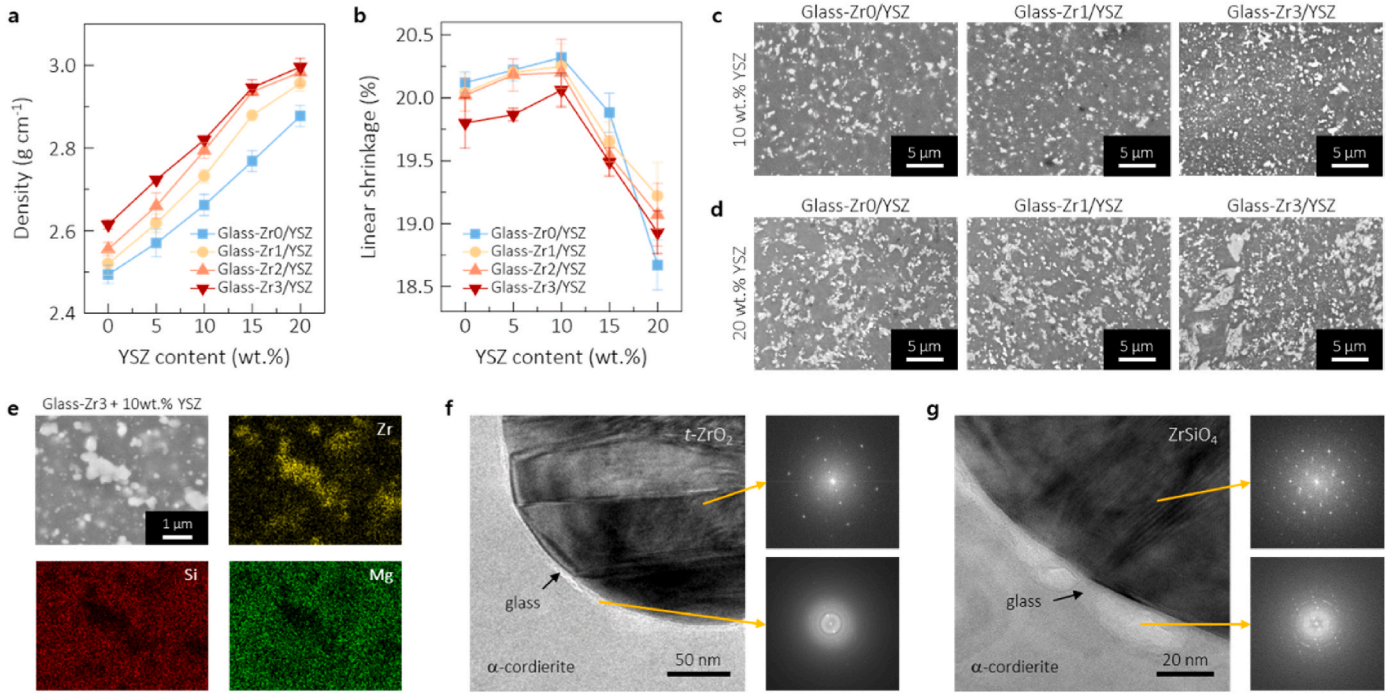

Fig. 3. (a,b) Variations in (a) fired density and (b) linear shrinkage of the composite samples sintered at 1050 °C for 2 h. (c,d) Surface SEM images of the composite samples containing (c) 10 wt% and (d) 20 wt% YSZ fillers for the Glass-Zr0, Glass-Zr1, and Glass-Zr3, in which discrete bright-contrast phases are dispersed over the surfaces depending on both the zirconia content in the glasses and the YSZ filler content in the composites (note negligible porosity unlike that of typical cordierite/zirconia ceramic composites). (e) Highlighted SEM of Glass-Zr3/10 wt% YSZ with the elemental EDS mapping of Zr, Si, and Mg. (f,g) Highlighted TEM micrographs of (f) crystalline ZrO_2 in cordierite matrix with the SAED patterns of *t*-ZrO_2 (top) and amorphous glass (bottom), and (g) crystalline $ZrSiO_4$ in cordierite matrix with the corresponding patterns of $ZrSiO_4$ (top) and amorphous glass (bottom).

proportionally with the increments of ZrO_2 content in the glasses and composites because the density of zirconia itself is much higher than that of cordierite. In this regard, chasing the linear shrinkage may be indicative of the progress of densification. Obviously, the 10 wt% YSZ seemed to create the optimal densification of the composites with the higher shrinkage values for all the glasses. There have been the optimized contents of fillers for best densification in the case of glass/ceramic composites as being associated with the effectiveness of the formation of glass networks vis viscous flow in the presence of dispersed fillers [47,48].

Fig. 3(c and d) shows the surface SEM images of the selected composite samples sintered at 1050 °C for 2 h (see Fig. S9 for more SEM images of other composites). All the samples demonstrate a well-densified microstructure with negligible porosity—a common characteristic of glass–ceramic structures, wherein the low-temperature-softening glass is responsible for filling voids during the initial viscous movements in the presence of dispersed YSZ fillers. In conjunction with the phase evolution observed in the previous XRD patterns, the dissimilar-contrast portions of the composite surfaces may be correlative to the evolved crystalline phases. For instance, the white homogeneously distributed particles likely correspond to zirconia phase in the dark background of the cordierite matrix phase. For the composite structures with the higher YSZ content, additional grey-contrast areas appear dominantly—possibly zircon phases. The energy dispersive spectroscopy (EDS) elemental mapping images of Fig. 3(e) demonstrate the dominant presence of Zr in the precipitates, compared to the matrix phase of cordierite. Fig. S10 shows the plots of each elemental peaks for the representative two regions of the matrix and precipitates, ensuring that the precipitates are based on Zr-rich phase. Overall, the white and grey portions tended to be more extensive with the higher contents of zirconia in the composites, consistent with the stronger peaks for the zirconia and zircon phases with the higher YSZ contents in the XRD

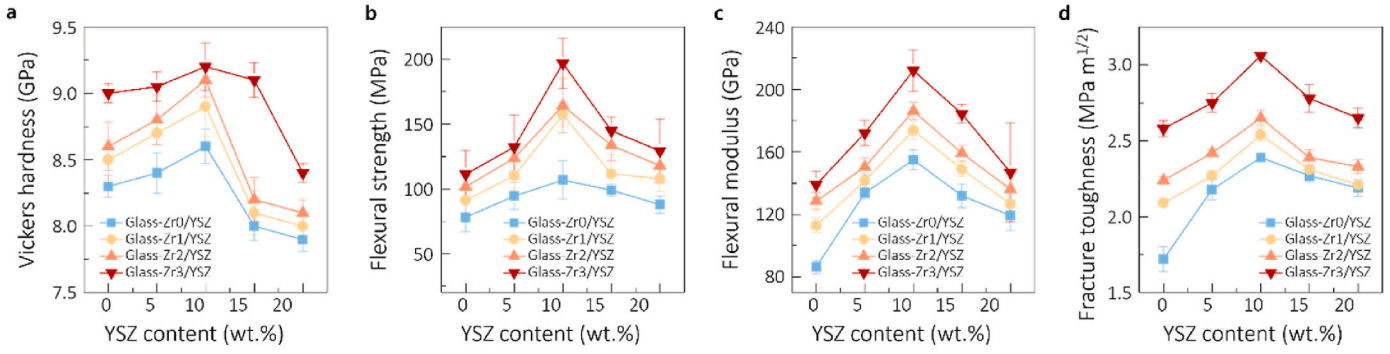

Fig. 4. (a) Vickers hardness, (b) flexural strength, (c) flexural modulus, and (d) fracture toughness of the composite samples containing different YSZ contents from 0 to 20 wt% for the Glass-Zr0, Glass-Zr1, Glass-Zr2, and Glass-Zr3, wherein all the trends in the mechanical properties suggest that 10 wt% YSZ in Glass-Zr3 is the best composition in terms of viable mechanical characteristics for the covers of mobile phones.

Table 1
Comparison of our best values with the reported mechanical properties of cordierite-based composites, indicating the excellency of our composite system. Note that most of the reported cases are based on crystalline cordierite requiring high-temperature densification greater than 1200 °C.

Composition	Sintering condition	Vickers hardness (GPa)	Flexural strength (MPa)	Flexural modulus (GPa)	Fracture toughness (MPa $m^{1/2}$)	Ref.
Cordierite (ceramic)/30 wt% mullite	1450 °C, 2 h	9.0	N/A	137	1.9	[56]
Cordierite (ceramic)/10 wt% *m*-ZrO_2	1250 °C, 1 h	8.1	92.5	119.2	1.9	[16]
Cordierite (ceramic)/10 vol% *m*-ZrO_2	1300 °C, 4h	N/A	160	N/A	2.4	[54]
Cordierite (ceramic)/6 wt% *t*-ZrO_2	1375 °C, 2 h	N/A	131	N/A	1.9	[15]
Cordierite (ceramic)/20 wt% TiC	1350 °C, 2h	N/A	158	N/A	N/A	[57]
Cordierite (glass)/20 vol% SiC	1200 °C, 0.5 h	N/A	~95	N/A	2.7	[58]
Cordierite (ceramic)/10 wt% $ZrSiO_4$	1300 °C, 0.5 h	8.3	~98	~112	1.5	[59]
Cordierite (ceramic)/12 vol% $ZrSiO_4$	1300 °C, 1h	6.4	N/A	N/A	N/A	[60]
Cordierite (ceramic)/30 wt% mullite	1300 °C, 2 h	N/A	106	81	N/A	[61]
Cordierite (ceramic)/60 wt% SiC	1360 °C, 2 h	N/A	54.6	N/A	N/A	[62]
Cordierite (ceramic)/20 wt% Ti_3SiC_2	1350 °C, 2 h	N/A	180	N/A	N/A	[63]
Cordierite (ceramic)/10 wt% Spodumene/15 wt% Zircon	1360 °C, 2 h	N/A	~100	N/A	N/A	[64]
Cordierite (ceramic)/9.5 wt% Spodumene/5 wt% Al_2SiO_5	1400 °C, 2h	N/A	104.9	N/A	N/A	[65]
Cordierite (ceramic)/10 wt% TiO_2	1300 °C, 3 h	6.5	158.5	N/A	~3.0	[66]
Cordierite (ceramic)/40 wt% Mica	1200 °C, 2 h	4.7	142.7	N/A	2.9	[67]
Cordierite (ceramic)/5 wt% h-BN	1350 °C, 1.5 h	8.5	N/A	N/A	N/A	[68]
Cordierite (ceramic)/40 wt% AlN	1400 °C, 4 h	N/A	175	~80	0.3	[69]
Cordierite (ceramic)/spinel/6 wt% NiO	1200 °C, 2h	8.3	N/A	N/A	N/A	[70]
Cordierite (ceramic)/24 vol% CaO–B_2O_3–SiO_2 glass	1200 °C, 2h	5.7	N/A	N/A	N/A	[71]
Cordierite (Glass-Zr3)/10 wt% YSZ	1050 °C, 2 h	9.2	196.8	212.1	3.1	This work

patterns. Notably, cordierite ceramic/zirconia composites exhibited considerable porosity, even at a high sintering temperature of 1400 °C in literature [49,50], supporting the advantages of our glass-based composite system. In addition, the presence of crystalline phases of ZrO_2 and $ZiSiO_4$ were confirmed by the TEM observation as seen in Fig. 3(f and g). The TEM images represent the interfacial regions around the crystallized *t*-ZrO_2 (Fig. 3(f)) and $ZrSiO_4$ (Fig. 3(g)) phases in the glass-ceramic matrix, which are along with the corresponding selected area electron diffraction (SAED) patterns. It is interestingly observed that the surfaces of the crystalline phases were surrounded with the glassy phase. The observation is plausible because the cordierite glass is supposed to wet the surface of YSZ filler particles in the initial stage of densification and the formation of $ZrSiO_4$ likely proceeds through the interfacial reactions.

Fig. 4(a–d) shows the mechanical properties of the glass and composite samples sintered at 1050 °C as a function of the YSZ content, specifically the Vickers hardness, flexural strength, flexural modulus, and fracture toughness. The actual values are listed in Table S1, which were taken as average ones from the multiple measurements. The mechanical values pertain to typical ranges for these parameters reported for cordierite-based glass–ceramics or related composite materials. All the varying tendencies with the YSZ contents were identical, showing peak values in the case of the composites composed of Glass-Zr3 (containing the highest amount of ZrO_2) and 10 wt% YSZ. Notably, the fracture strength and toughness of cordierite ceramic/zirconia ceramic composites were reported to increase up to the maximum content of zirconia, typically up to 40 wt% [51,52]. The enhanced mechanical behavior in the ceramic/ceramic composites was attributed to the toughening effect in microstructures with the transformation of tetragonal to monoclinic zirconia and the stronger presence of zircon [53,54].

In our system, the mechanism for the enhanced toughening must be similar to that reported previously because these phases are also widespread over the samples depending on the contents of zirconia in the glasses and composites. Only a noticeable difference lies in the fact that the optimal densification was attained with the optimal filler content dispersed in the glass matrix, especially without producing porosity that was seriously observed in the reported ceramic/ceramic composites [18,55]. Note that the crystallization of the phases in our system happens after densification of the cordierite glass, as confirmed by the TMA and DTA curves. Although the optimal content of the YSZ filler was apparent merely with 10 wt%, the peak values attained in composite structures were outstanding. For example, the best average Vickers hardness of ~9.2 GPa for the Glass-Zr3/10 wt% YSZ sample corresponds to a substantial improvement over the ~8.3 GPa for Glass-Zr0 without YSZ. With the simultaneous benefits from zirconia both in the glass (as a constituent) and composites (as a filler), the highest average flexural strength of ~196.8 MPa for the Glass-Zr3/10 wt% YSZ sample is very encouraging considering the low sintering temperature. The best flexural strength means an increment by ~152 % relative to ~78.1 MPa for the Glass-Zr0 sample (with no YSZ filler). This same optimized composite exhibited a flexural modulus of ~212.1 GPa and fracture toughness of ~3.06 MPa $m^{1/2}$, indicating highly competitive values compared with those of similar composite cases. The best values obtained for the Glass-Zr3/10 wt% YSZ sample were compared with the corresponding outcomes reported for cordierite-based composites as presented in Table 1 [15,16,54,56–71]. The comparison indicates the excellency of our composite system in terms of all the major mechanical parameters. Note that most of reported composites were densified in the temperature

Table 2
Dielectric properties at GHz, measured by the Hakki-Coleman method.

Composition	Frequency *f* (GHz)	Dielectric constant *k*	Quality factor *Q*	$Q \times f$ (GHz)	Loss tangent
Glass-Zr0	8.97	4.97	1822.7	16348.3	5.49×10^{-4}
Glass-Zr1	8.91	4.99	1901.0	16930.5	5.26×10^{-4}
Glass-Zr2	9.22	5.11	1590.4	14670.1	6.29×10^{-4}
Glass-Zr3	9.67	5.25	913.3	8828.2	10.9×10^{-4}
Glass-Zr0/10 wt% YSZ	9.37	5.34	1949.7	18274.7	5.13×10^{-4}
Glass-Zr1/10 wt% YSZ	8.91	5.36	1564.6	13948.2	6.39×10^{-4}
Glass-Zr2/10 wt% YSZ	8.89	5.50	1517.6	13484.5	6.59×10^{-4}
Glass-Zr3/10 wt% YSZ	9.12	5.57	1351.7	12326.4	7.40×10^{-4}

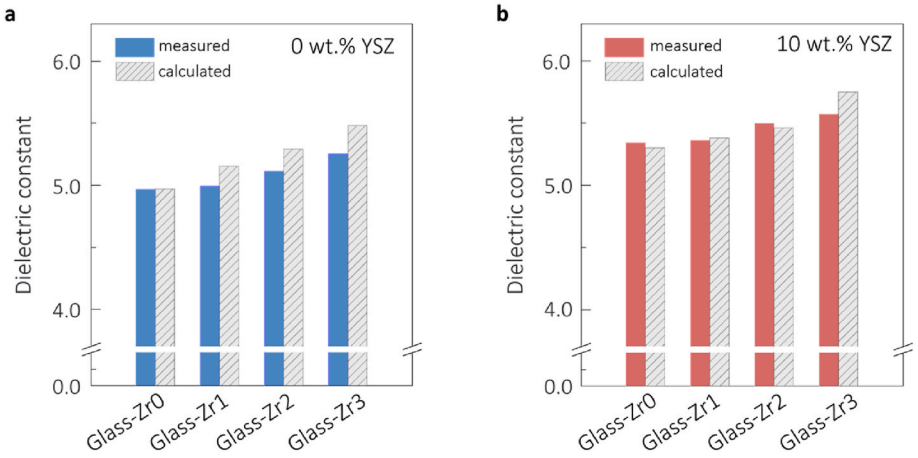

Fig. 5. (a,b) Changes in dielectric constant of the composite samples for different glasses in the cases of (a) no filler and (b) 10 wt% YSZ filler, in which the measured and calculated values are plotted per each case. Note that the calculated values were based on the volumetric mixture rule considering the contribution of each phase to overall dielectric constant on the basis of its volume fraction with the assumption of 10 vol% residual glass.

range of 1200–1450 °C. A noteworthy result of flexural strength was 160 MPa achieved for a cordierite ceramic/10 vol% *m*-ZrO_2 composite sintered at 1300 °C for 4 h [54]. For the cover of mobile phones, the hardness and flexural strength, which indicate the resistance against scratching and mechanical shock, respectively, are the major concern for commercialization as introduced earlier.

Dielectric properties of the composites were examined to confirm the suitability for the phone cover applications. Table 2 presents all dielectric values, including dielectric constant, loss tangent, and quality factor Q with the measured frequency f, for the glass and composite samples. As expected, dielectric constant was raised with the relative contents of zirconia in the glasses and composites as the dielectric constant of zirconia is much higher than that of cordierite [72]. All permittivity values met the original target of low dielectric constant for 6G communication networks. Based on the XRD analysis of Fig. 2(e), the effective dielectric constant was evaluated according to the volumetric mixture rule counting the contribution of each phase to overall dielectric constant as being expressed with the relation of effective dielectric constant k_{eff} [73,74]:

$$k_{eff} = \sum_{i=1}^{N} v_i k_i$$

where N is the total number of crystalline phases, v_i is the volume fraction of i phase, and k_i is the dielectric constant of i phase. With the consideration of dielectric constant of each crystalline phase, i.e., 25 for *t*-ZrO_2 [75], 17.9 for *m*-ZrO_2 [75], and 7.4 for $ZrSiO_4$ [76], the calculated k_{eff} values were plotted with the measured values for the cases of no filler and 10 wt% YSZ samples as seen in Fig. 5 with the assumption of 10 vol % residual glass. The calculated values are closely approximated with the measured values. For example, the composite of Glass-Zr2 with 10 wt% YSZ filler demonstrated an estimated k_{eff} of 5.46 that is close to the measured 5.50. The calculation results fully support the observed trend of increasing dielectric constant of composites with the higher contents of zirconia in the glasses and composites. Dielectric loss tangent of the glass and composite samples at microwave frequencies remained consistently low, on the order of 10^{-4}, when subjected to microwave frequencies. For the optimal Glass-Zr3/10 wt% YSZ sample, k of ~5.57 and loss of $\sim 7.40 \times 10^{-4}$ were obtained with a high $Q \times f$ value of ~12, 326 GHz, thus indicating the suitability as a functional mobile phone cover.

4. Conclusion

Unprecedented composites comprising cordierite glass–ceramics with YSZ ceramic fillers were proven to be viable as mobile phone covers for next-generation communications, with the outstanding mechanical properties optimized with the contents of nucleating ZrO_2 in the glasses and YSZ filler in the composites. The presence of ZrO_2 in the glass facilitated earlier crystallization and induced better mechanical behavior. The YSZ fillers in the crystallizable system more effectively enhanced the mechanical properties while maintaining dielectric constant low. As a highlight, our best mechanical results, Vickers hardness of 9.2 GPa, flexural strength of 196.8 MPa, flexural modulus of 212.1 GPa, and fracture toughness of 3.1 MPa $m^{1/2}$, which were achieved for the optimized glass–ceramic/ceramic composite consisting of the highest ZrO_2-containing glass with 10 wt% YSZ, exceed the reported values for any cordierite-based composites. As expected, dielectric properties at GHz were suitable for the 6G communication applications with the dependence of dielectric properties on the glass and composite compositions. The experimental dielectric constant was well approximated with the calculated permittivity as a result of applying the volumetric mixture rule considering the contribution of each phase to the overall dielectric constant on the basis of volume fraction. The achievements may be a good benchmark for new physical applications demanding adjustable mechanical and electrical properties.

CRediT authorship contribution statement

Ji Yeon Kim: Writing – original draft, Investigation, Formal analysis. **Seok Won Choi:** Investigation, Formal analysis. **Kwan Sik Park:** Validation, Investigation. **Yong-yi Kim:** Resources, Investigation. **Taehong Kim:** Resources, Investigation. **Sang Bong Lee:** Investigation, Conceptualization. **Jongsu Lee:** Investigation, Conceptualization. **Seok Eun Kwon:** Investigation. **Young-Kook Lee:** Supervision, Resources. **Do-Kyun Kwon:** Supervision, Resources. **Sang-Jin Lee:** Supervision, Resources. **Yong Soo Cho:** Writing – review & editing, Supervision, Funding acquisition.

Declaration of competing interest

The authors declare that they have no known competing financial interests or personal relationships that could have appeared to influence the work reported in this paper.

Acknowledgment

This work was financially supported by an independent research and development project at Samsung Electronics Co., Ltd.

Appendix A. Supplementary data

Supplementary data to this article can be found online at https://doi.org/10.1016/j.ceramint.2024.06.390.

References

[1] C. Feng, Y. Wu, Q. Li, T. He, Q. Cao, X. Li, Y. Xiao, J. Lin, X. Zhu, X. Zhang, A novel hollow-tube-biphasic-whisker-modified calcium phosphate ceramics with simultaneously enhanced mechanical strength and osteogenic activity, Adv. Funct. Mater. 32 (2022) 2204974.

[2] X. Yang, Z. Su, Q. Huang, X. Fang, L. Chai, Microstructure and mechanical properties of C/C–ZrC–SiC composites fabricated by reactive melt infiltration with Zr, Si mixed powders, J. Mater. Sci. Technol. 29 (2013) 702–710.

[3] D. Sciti, L. Silvestroni, V. Medri, S. Guicciardi, Pressureless sintered in situ toughened ZrB_2–SiC platelets ceramics, J. Eur. Ceram. Soc. 31 (2011) 2145–2153.

[4] T. Masaki, K. Sinjo, Mechanical properties of highly toughened ZrO_2–Y_2O_3, Ceram. Int. 13 (1987) 109–112.

[5] T. Masaki, Mechanical properties of toughened ZrO_2–Y_2O_3 Ceramics, J. Am. Ceram. Soc. 69 (1986) 638–640.

[6] J. Kondoh, H. Shiota, K. Kawachi, T. Nakatani, Yttria concentration dependence of tensile strength in yttria-stabilized zirconia, J. Alloys Compd. 365 (2004) 253–258.

[7] Y.S. Cho, D.T. Hoelzer, W.A. Schulze, V.R.W. Amarakoon, Cordierite-based dielectric thick films on an oxidized copper layer: microstructural evidence of copper diffusion, J. Am. Ceram. Soc. 82 (1999) 1949–1952.

[8] Z. Li, Z. Liu, F. Dufosse, L. Yan, D.Y. Wang, Interfacial engineering of layered double hydroxide toward epoxy resin with improved fire safety and mechanical property, Compos. Pt. B-Eng. 152 (2018) 336–346.

[9] H. Ohsato, J. Varghese, A. Kan, J.S. Kim, I. Kagomiya, H. Ogawa, M.T. Sebastian, H. Jantunen, Volume crystallization and microwave dielectric properties of indialite/cordierite glass by TiO_2 addition, Ceram. Int. 47 (2021) 2735–2742.

[10] M.A. Camerucci, G. Urretavizcaya, A.L. Cavalieri, Sintering of cordierite based materials, Ceram. Int. 29 (2003) 159–168.

[11] W. Wang, Z. Shi, X. Wang, W. Fan, The phase transformation and thermal expansion properties of cordierite ceramics prepared using drift sands to replace pure quartz, Ceram. Int. 42 (2016) 4477–4485.

[12] S. Li, C. Bao, W. Dong, R. Liu, Phase evolution and properties of porous cordierite ceramics prepared by cordierite precursor pastes based on supportless stereolithography, J. Alloys Compd. 922 (2022) 166295.

[13] C.N. Djangang, C. Tealdi, A.S. Cattaneo, P. Mustarelli, E. Kamseu, C. Leonelli, Cold-setting refractory composites from cordierite and mullite–cordierite design with geopolymer paste as binder: thermal behavior and phase evolution, Mater. Chem. Phys. 154 (2015) 66–77.

[14] S. Liu, H. Zhang, B. Zhang, X. Zhong, J. Ma, F. Ye, Fabrication and properties of cordierite based glass/AlN composites by sol-gel and pressureless sintering, Ceram. Int. 42 (2016) 7253–7258.

[15] C. Zhang, Z. Luo, J. Cao, J. Yuan, M. Jiang, P. Wang, C. Liu, C.P. Jiang, Z. Chen, Mechanical reinforcement of 3D printed cordierite–zirconia composites, Ceram. Int. 48 (2022) 5636–5645.

[16] F.A. Costa Oliveira, J. Cruz Fernandes, Mechanical and thermal behaviour of cordierite–zirconia composites, Ceram. Int. 28 (2002) 79–91.

[17] A.D. Gupta, P.S. Sen, M.K. Sinha, M.K. Basu, Effect of ZrO_2 addition on strength and dilation behaviour of cordierite ceramics, J. Mater. Sci. Lett. 13 (1994) 332–334.

[18] M. Di Maro, D. Duraccio, G. Malucelli, M.G. Faga, High density polyethylene composites containing alumina-toughened zirconia particles: mechanical and tribological behavior, Compos. Pt. B-Eng. 217 (2021) 108892.

[19] I. Ahmad, M. Islam, N. Al Habis, S. Parvez, Hot-pressed graphene nanoplatelets or/and zirconia reinforced hybrid alumina nanocomposites with improved toughness and mechanical characteristics, J. Mater. Sci. Technol. 40 (2020) 135–145.

[20] Y.H. Jo, M.S. Kang, K.W. Chung, Y.S. Cho, Chemical stability and dielectric properties of RO–La_2O_3–B_2O_3 (R = Ca, Mg, Zn)-based ceramics, Mater. Res. Bull. 43 (2008) 361–369.

[21] I.J. Choi, Y.S. Cho, Effects of various oxide fillers on physical and dielectric properties of calcium alumnoborosilicate-based dielectrics, J. Electroceram. 23 (2009) 185–190.

[22] K.P. Hong, I.J. Choi, J.W. Jung, H.R. Choi, Y.S. Cho, J. Kwak, D.H. Kang, Densification, crystallization and dielectric properties of AlN, BN and Si_3N_4 filler-containing LTCC materials, Int. J. Appl. Ceram. Technol. 10 (2013) E25–E32.

[23] S.M. Lee, Y.H. Jo, H.E. Kim, B.C. Mohanty, Y.S. Cho, Barium neodymium titanium borate glass-based high k dielectrics, J. Am. Ceram. Soc. 95 (2012) 1356–1359.

[24] K. Niihara, R. Morena, D.P.H. Hasselman, Evaluation of K_{Ic} of brittle solids by the indentation method with low crack-to-indent ratios, J. Mater. Sci. Lett. 1 (1982) 13–16.

[25] B.W. Hakki, P.D. Coleman, A dielectric resonator method of measuring inductive capacities in the millimeter range, IRE Trans. Microw. Theory Tech. 8 (4) (1960) 402–410.

[26] D. Kajfez, P. Guillon, Dielectric Resonators, Artech House, Norwood, 1986.

[27] Y.S. Cho, W.A. Schulze, V.R.W. Amarakoon, Crystallization kinetics and properties of nonstoichiometric cordierite-based thick-film dielectrics, J. Am. Ceram. Soc. 82 (1999) 3186–3192.

[28] Y.S. Cho, D.T. Hoelzer, W.A. Schulze, V.R.W. Amarakoon, Crystallization and microstructural evolution of cordierite-based thick film dielectrics, Acta Mater. 46 (1998) 6421–6430.

[29] I. Wadsworth, J. Wang, R. Stevens, Zirconia toughened cordierite, J. Mater. Sci. 25 (1990) 3982–3989.

[30] A. Nastic, A. Merati, M. Bielawski, M. Bolduc, O. Fakolujo, M. Nganbe, Instrumented and Vickers indentation for the characterization of stiffness, hardness and toughness of zirconia toughened Al_2O_3 and SiC armor, J. Mater. Sci. Technol. 31 (2015) 773–783.

[31] N. Rendtorff, L. Garrido, E. Aglietti, Mullite–zirconia–zircon composites: properties and thermal shock resistance, Ceram. Int. 35 (2009) 779–786.

[32] Y. Demirci, E. Günay, Crystallization behavior and properties of cordierite glass–ceramics with added boron oxide, J. Ceram. Process. Res. 12 (2011) 352–356.

[33] S. Mei, J. Yang, J.M.F. Ferreira, Microstructural evolution in sol–gel derived P_2O_5-doped cordierite powders, J. Eur. Ceram. Soc. 20 (2000) 2191–2197.

[34] S. Kumar, K. Singh, D. Kumar, SiO_2/B_2O_3 glass formers effect on transparency and mechanical properties of soda-lime borosilicate glasses for automobile applications, J. Non-Cryst. Solids 618 (2023) 122530.

[35] J. Wu, S. Hwang, Effects of (B_2O_3, P_2O_5) additives on microstructural development and phase-transformation kinetics of stoichiometric cordierite glasses, J. Am. Ceram. Soc. 83 (2000) 1259–1265.

[36] J.W. Cao, Y.H. Li, K.M. Liang, Effect of P_2O_5 on evolution of microstructure of MgO–Al_2O_3–SiO_2 glass ceramics, Adv. Appl. Ceram. 108 (2009) 352–357.

[37] Y.J. Sue, P. Shen, S.Y. Chen, H.Y. Lu, Spherulitic growth from a phase-separated vitreous matrix in a cordierite–y-stabilized zirconia glass-ceramic, J. Am. Ceram. Soc. 74 (1991) 85–91.

[38] W. Yu, S. Cao, J. Wang, Z. Zhang, J. Han, C. Liu, J. Ruan, Crystallization mechanisms of cordierite glass–ceramics with "surface-center" crystallization behavior, J. Eur. Ceram. Soc. 41 (2021) 6708–6721.

[39] I.W. Donald, The crystallization kinetics of a glass based on the cordierite composition studied by DTA and DSC, J. Mater. Sci. 30 (1995) 904–915.

[40] E.F. Krivoshapkina, P.V. Krivoshapkin, A.A. Vedyagin, Synthesis of Al_2O_3–SiO_2–MgO ceramics with hierarchical porous structure, J. Adv. Ceram. 6 (2017) 11–19.

[41] H.I. Hsiang, S.W. Yung, C.C. Wang, Crystallization, densification and dielectric properties of CaO–MgO–Al_2O_3–SiO_2 glass with ZrO_2 as nucleating agent, Mater. Res. Bull. 60 (2014) 730–737.

[42] L. Zhu, M. Wang, Y. Xu, X. Zhang, P. Lu, Dual effect of ZrO_2 on phase separation and crystallization in Li_2O–Al_2O_3–SiO_2–P_2O_5 glasses, J. Am. Ceram. Soc. 105 (2022) 5698–5710.

[43] E.H. Sun, T. Kusunose, T. Sekino, K. Niihara, Fabrication and characterization of cordierite/zircon composites by reaction sintering: formation mechanism of zircon, J. Am. Ceram. Soc. 85 (2002) 1430–1434.

[44] M.S. Kumar, A.E. Perumal, T.R. Vijayaram, G. Senguttuvan, Processing and characterization of pure cordierite and zirconia-doped cordierite ceramic composite by precipitation technique, Bull. Mater. Sci. 38 (2015) 679–688.

[45] L. Fu, B. Li, G. Xu, J. Huang, H. Engqvist, W. Xia, Size-driven phase transformation and microstructure evolution of ZrO_2 nanocrystallites associated with thermal treatments, J. Eur. Ceram. Soc. 41 (2021) 5624–5633.

[46] Q. Chen, Y. Chang, C. Shao, J. Zhang, J. Chen, M. Wang, Y. Long, Effect of grain size on phase transformation and photoluminescence property of the nanocrystalline ZrO_2 powders prepared by sol–gel method, J. Mater. Sci. Technol. 30 (2014) 1103–1107.

[47] M.F. Zawrah, E.M.A. Hamzawy, Effect of cristobalite formation on sinterability, microstructure and properties of glass/ceramic composites, Ceram. Int. 28 (2002) 123–130.

[48] A.A. El Kheshen, M.F. Zawrah, Sinterability, microstructure and properties of glass/ceramic composites, Ceram. Int. 29 (2003) 251–257.

[49] M.M.S. Sanad, M.M. Rashad, E.A. Abdel Aal, M.F. El Shahat, K. Powers, Structural, microstructure, mechanical and electrical properties of porous Zr^{4+}-cordierite ceramic composites, J. Mater. Eng. Perform. 23 (2014) 867–874.

[50] R. Švinka, V. Svinka, J. Bobrovik, Modification of porous cordierite ceramic, Key Eng. Mater. 721 (2017) 322–326.

[51] H.M. Jang, Surface precipitation route for the development of cordierite-zirconia composites, J. Am. Ceram. Soc. 78 (1995) 723–727.

[52] M. Awano, H. Takagi, Synthesis of cordierite and cordierite-$ZrSiO_4$ composite by colloidal processing, J. Mater. Sci. 29 (1994) 412–418.

[53] M. Mamivand, M. Asle Zaeem, H. El Kadiri, Phase field modeling of stress-induced tetragonal-to-monoclinic transformation in zirconia and its effect on transformation toughening, Acta Mater. 64 (2014) 208–219.

[54] Y. Oh, T. Oh, H. Jung, Microstructure and mechanical properties of cordierite ceramics toughened by monoclinic ZrO_2, J. Mater. Sci. 26 (1991) 6491–6495.

[55] B.S. Vasile, E. Andronescu, C. Ghitulica, O.R. Vasile, L. Curechiu, R. Scurtu, E. Vasile, R. Trusca, L. Pall, V. Aldica, Microstructure and electrical properties of zirconia and composite nanostructured ceramics sintered by different methods, Ceram. Int. 39 (2013) 2535–2543.

[56] M.A. Camerucci, G. Urretavizcaya, A.L. Cavalieri, Mechanical behavior of cordierite and cordierite–mullite materials evaluated by indentation techniques, J. Eur. Ceram. Soc. 21 (2001) 1195–1204.

[57] Y. Liu, Y. Li, F. Luo, X. Su, J. Xu, J. Wang, Y. Qu, Y. Shi, Mechanical, dielectric and microwave absorption properties of TiC/cordierite composite ceramics, J. Mater. Sci. Mater. Electron. 28 (2017) 12115–12121.

[58] R. Chaim, V. Talanker, Microstructure and mechanical properties of SiC platelet/cordierite glass–ceramic composites, J. Am. Ceram. Soc. 78 (1995) 166–172.

[59] M. Valášková, G. Simha Martynková, J. Zdrálková, J. Vlček, P. Matějková, Cordierite composites reinforced with zircon arising from zirconium–vermiculite precursor, Mater. Lett. 80 (2012) 158–161.

[60] F.A. Costa Oliveira, J.A. Franco, J. Cruz Fernandes, D. Dias, Newly developed cordierite–zircon composites, Br. Ceram. Trans. 101 (1) (2002) 14–21.
[61] E. Ozel, S. Kurama, Effect of the processing on the production of cordierite–mullite composite, Ceram. Int. 36 (2010) 1033–1039.
[62] S. Zhu, S. Ding, H. Xi, Q. Li, R. Wang, Preparation and characterization of SiC/cordierite composite porous ceramics, Ceram. Int. 33 (2007) 115–118.
[63] Y. Liu, F. Luo, J. Su, W. Zhou, D. Zhu, Z. Li, Enhanced mechanical, dielectric and microwave absorption properties of cordierite based ceramics by adding Ti_3SiC_2 powders, J. Alloys Compd. 619 (2015) 854–860.
[64] J. Wu, C. Hu, C. Ping, X. Xu, W. Xiang, Preparation and corrosion resistance of cordierite–spodumene composite ceramics using zircon as a modifying agent, Ceram. Int. 44 (2018) 19590–19596.
[65] C. Hu, J. Wu, X. Xu, P. Chen, Investigating the effect of andalusite on mechanical strength and thermal shock resistance of cordierite–spodumene composite ceramics, Ceram. Int. 44 (2018) 3240–3247.
[66] S.K. Marikkannan, E.P. Ayyasamy, Synthesis, characterisation and sintering behaviour influencing the mechanical, thermal and physical properties of cordierite-doped TiO_2, J. Mater. Res. Technol. 2 (2013) 269–275.
[67] S. Taruta, T. Hayashi, K. Kitajima, Preparation of machinable cordierite/mica composite by low-temperature sintering, J. Eur. Ceram. Soc. 24 (2004) 3149–3154.
[68] C. Tekin, E. Ercenk, Ş. Yılmaz, A.Ş. Demirkıran, Characterization of cordierite based h-BN doped ceramics as an electronic substrate/circuit board material, Int. J. Appl. Ceram. Technol. 19 (2022) 3461–3479.
[69] J. Ma, K. Liao, P. Hing, Effect of aluminum nitride on the properties of cordierite, J. Mater. Sci. 35 (16) (2000) 4137–4141.
[70] H.E.H. Sadek, M.F. Zawrah, R.M. Khattab, H.H. Abo Almaged, Effect of CuO, NiO, MnO_2 and sintering temperature on the formation of cordierite–spinel composites processed by direct coagulation casting, J. Mater. Sci. Mater. Electron. 34 (2023) 1196.
[71] G. Chen, L. Tang, J. Cheng, M. Jiang, Synthesis and characterization of CBS glass/ceramic composites for LTCC application, J. Alloys Compd. 478 (2009) 858–862.
[72] D. Vanderbilt, X. Zhao, D. Ceresoli, Structural and dielectric properties of crystalline and amorphous ZrO_2, Thin Solid Films 486 (2005) 125–128.
[73] A. Tumarkin, N. Tyurnina, N. Mukhin, Z. Tyurnina, O. Sinelshchikova, A. Gagarin, E. Sapego, Y. Kretser, Glass–ceramic ferroelectric composite material $BaTiO_3$/KFeSi for microwave applications, Compos. Struct. 281 (2022) 114992.
[74] M. Lay, S. Meng, H. Ismail, T.S. Huat, M. Todo, Changes in the dielectric constant of interphase volume in polyimide–ceramic nanocomposites: a power law model approach, J. Appl. Polym. Sci. 139 (2022) 51600.
[75] Y. Oh, V. Bharambe, B. Mummareddy, J. Martin, J. McKnight, M.A. Abraham, J. M. Walker, K. Rogers, B. Conner, P. Cortes, E. Macdonald, J.J. Adams, Microwave dielectric properties of zirconia fabricated using NanoParticle Jetting, Addit. Manuf. 27 (2019) 586–594.
[76] J. Varghese, T. Joseph, M.T. Sebastian, $ZrSiO_4$ ceramics for microwave integrated circuit applications, Mater. Lett. 65 (2011) 1092–1094.